ENVIRONMENTAL RESEARCH
LETTERS

LETTER • OPEN ACCESS

Slowdown and reversal of terrestrial near-surface wind speed and its future changes over eastern China

IOP Publishing Environ. Res. Lett. 16 (2021) 034028 https://doi.org/10.1088/1748-9326/abe2cd

ENVIRONMENTAL RESEARCH
LETTERS

OPEN ACCESS

RECEIVED
1 August 2020

REVISED
3 December 2020

ACCEPTED FOR PUBLICATION
3 February 2021

PUBLISHED
22 February 2021

LETTER

Slowdown and reversal of terrestrial near-surface wind speed and its future changes over eastern China

Jinlin Zha[1,2], Cheng Shen[3], Deming Zhao[1], Jian Wu[2] and Wenxuan Fan[2]

[1] CAS Key Laboratory of Regional Climate and Environment for Temperate East Asia, Institute of Atmospheric Physics, Chinese Academy of Sciences, Beijing 100029, People's Republic of China
[2] Key Laboratory of Atmospheric Environment and Processes in the Boundary Layer over the Low-Latitude Plateau Region, Department of Atmospheric Science, Yunnan University, Kunming 650091, People's Republic of China
[3] Gaochun Meteorological Bureau, Nanjing 211300, People's Republic of China

E-mail: wujian@ynu.edu.cn

Keywords: CMIP6, forward stepwise regression algorithm, large-scale ocean-atmosphere circulations, reversal, near-surface wind speed

Supplementary material for this article is available online

Abstract

A recovery of near-surface wind speed (SWS) in the last decade has been reported over China; nevertheless, the contributions of large-scale ocean-atmosphere circulations (LOACs) to the SWS changes are rarely investigated. In this study, the turning point (TP) of the terrestrial stilling was validated over eastern China for 1979–2017. Furthermore, a forward stepwise regression algorithm was used to assess the contribution of LOACs to SWS changes. The results revealed that the TP of the SWS reversal occurred in approximately 2011 during the study period. Mean annual and seasonal SWSs exhibited decreases before the TP, with the largest decrease in spring (-0.134 ± 0.014 m s^{-1} decade^{-1}), while SWSs increased after the TP, most strongly in autumn (0.377 ± 0.053 m s^{-1} decade^{-1}). The SWS decrease before the TP and increase after the TP were caused by the decreasing and increasing frequencies of strong windy days (>75th percentile of SWS), respectively. The effects of LOACs on the long-term changes of SWS were pronounced. The contributions of LOACs to the decreasing and increasing trends of SWSs were >60.0%, with the exception of autumn. The projected SWSs exhibited increases in the near-term (2021–2040) for the low-emission scenarios (e.g. Shared Socioeconomic Pathway 245). For the mid-term and long-term projections, the SWSs still displayed a downward trend, which was mainly attributed to the reduction of strong windy days. Consequently, the present SWS recovery in the recent decade may be only expected to last for a short amount of time before winds start decreasing again.

1. Introduction

Near-surface wind speed (SWS) is an important parameter in the study of atmospheric dynamics and climate change. The investigation of SWS variations facilitates the understanding of atmospheric circulation and improves the ability of climate analysis and prediction. SWS exerts a significant effect on air quality, wind energy, and evaporation (McMahon *et al* 2013, Zhang *et al* 2015). Especially, the SWS changes directly determine the development of wind energy resources, and SWS reductions of 1%–5% could cause wind energy losses of 1.7%–8.6% (He *et al* 2010). As the climate warms, the terrestrial SWS has decreased during the past several decades (Vautard *et al* 2010, McVicar *et al* 2012, Azorin-Molina *et al* 2014, Dadaser-Celik and Cengiz 2014, Kim and Paik 2015, Gilliland and Keim 2018). Roderick *et al* (2007) termed this decreasing trend in SWS 'stilling'.

Observed reductions in SWS have been reported in China (Jiang *et al* 2010, Li *et al* 2018a). Several studies have suggested that the weakening of SWS was caused by an increase in surface roughness attributed to the land use and cover change (Wu *et al* 2016, 2017, Zha *et al* 2016, 2017, 2020, Zhang *et al* 2019). Some researchers have also proposed that various large-scale ocean-atmosphere circulations (LOACs) are the drivers behind the SWS variations over China. Xu *et al* (2006) suggested that the reduction in SWS was associated with the East Asian monsoon. Chen *et al* (2013) and Lin *et al* (2013) proposed that the Arctic Oscillation (AO), Pacific Decadal Oscillation

(PDO), and El Niño/Southern Oscillation could be the primary drivers of SWS changes. As LOACs can induce pressure-gradient force (PGF) changes, some studies discovered that an essential cause of the weakening SWS was the lower-tropospheric PGF (Guo *et al* 2011, Wu *et al* 2018a). Many studies have shown that changes in LOACs can cause adjustments in global atmospheric circulation, generate stationary atmospheric waves, and lead to massive reorganizations of wind speed patterns (Naizghi and Ouarda 2017, Nchaba *et al* 2017, Zhang *et al* 2018). The relationship between these LOACs and long-term SWS changes over China has not been well established, however. Meanwhile, the contributions from the combined effects of different LOACs to SWS changes have not yet to be systematically evaluated.

Contrary to the reported SWS slowdown, a SWS recovery was also discovered during the last few decades (Zeng *et al* 2019). In China, the mean annual and seasonal SWSs in the southwestern part of the country have exhibited increasing trends after 2000 (Yang *et al* 2012). The strengthening of SWS was also observed over northwestern China from 1993 to 2005 and eastern China in winter from 2000 to 2011 (Li *et al* 2018b, Zha *et al* 2019). The original SWS series increased over all of China after the 1990s, although an increase in the detrended wind series was only observed in southern, southeastern, and northwestern China (Zhang and Wang 2020). Until now, however, the turning point (TP) of the SWS stilling has remained uncertain. Previous researchers have proposed that the potential causes of SWS recovery include (a) strengthening of the temperature difference between high and low latitudes (Li *et al* 2018b); (b) increase of sea-level pressure at high latitudes (Zha *et al* 2019); and (c) increase in the intensity of the Aleutian low over the North Pacific (Zhang and Wang 2020). The SWS changes include the combined influences of various LOACs, although there have only been a few studies that have estimated the contributions of primary LOACs to the recovery of SWSs over China. Consequently, in this study, we provide a comprehensive investigation of SWS reversal over eastern China. We attempted to answer the following questions: (a) When was the TP of the SWS decreases in the recent decade?; (b) What are the quantitative contributions of primary LOACs to the long-term changes in SWS?; and (c) Will the SWS recovery continue under different scenarios in the future? These issues have important implications for the evaluation and development of wind energy.

2. Datasets and methods

2.1. Datasets

Eastern China (15–55° N, 105–135° E) was selected as the study region due to its spatially dense network of meteorological observation stations and generally flat topography. The wind speed dataset was obtained from the China Meteorological Administration (CMA). The SWSs were measured with an anemometer 10 m above the surface. The setting, installation, and observation of each anemometer conformed to the CMA's technical regulation standard on weather observations (CMA 2003). The correct data, questionable data, and incorrect data were labeled with the quality codes 0, 1, and 2, respectively. This dataset was examined and calibrated by the CMA based on the homogeneity test, extreme test, and temporal consistency test. To obtain the homogeneous SWS at each station, the stations were selected based on the following criteria: (a) each station must be a national meteorological station; (b) total days of missing data accounted for <1% of the length of the total data series; and (c) the SWS must be accompanied by the quality code 0. Ultimately, 587 stations for the period 1979–2017 were selected (figure S1 (available online at stacks.iop.org/ERL/16/034028/mmedia)).

Climate indices (CIs) were selected to assess the influences of LOACs on SWS. These CIs included the Atlantic Meridional Mode (AMM) (Chiang and Vimont 2004), the AO (Higgins *et al* 2002), the East Asian Summer Monsoon (Li and Zeng 2002), the East Asian Winter Monsoon (EAWM) (Wang 2014), the Niño 3, Niño 3.4, and Niño 4 indices (Trenberth and Stepaniak 2001), the North Atlantic Oscillation (Barnston and Livezey 1987), the PDO (Mantua *et al* 1997), the solar flux (10.7 cm) (Moen and Brekke 1993), the South China Sea Summer Monsoon (Li and Zeng 2003), the Southern Hemisphere Annular Mode (Nan and Li 2003), the Tropical Northern Atlantic index (Enfield *et al* 1999), the Western Hemisphere Warm Pool (WHWP) (Wang and Enfield 2001), the Western Pacific Index (WPI) (Barnston and Livezey 1987), the Western Pacific Subtropical High Area (WPSHA), and the Western Pacific Subtropical High Intensity (Huang *et al* 2018) (table S1). These CIs exert considerable effects on climate changes in China and are informative in terms of the various fluctuations of LOACs. They have been widely used by the climate community.

Multimodel simulations and projections from the Coupled Model Intercomparison Project Phase 6 (CMIP6) were used. Projections from 23 models are analyzed. Meanwhile, Shared Socioeconomic Pathway (SSP) 245 (SS245) (+4.5 W m^{-2}; medium forcing middle-of-the-road pathway), SSP370 (+7.0 W m^{-2}; medium- to high-end forcing pathway), and SSP585 (+8.5 W m^{-2}; high-end forcing pathway) were considered (Cook *et al* 2020). The scenarios were the combination of SSPs and forcing levels of the Representative Concentration Pathways (RCPs) (Eyring *et al* 2016, O'Neill *et al* 2017, Wang *et al* 2019, Fan *et al* 2020). The monthly mean wind speed and the parent variant label 'r1i1p1f1' from each model were used. The outputs were interpolated onto

the same 1.0° × 1.0° resolution grid using bilinear interpolation.

2.2. Methods

A piecewise linear regression model (PLRM) was employed to quantify the TP. A PLRM is capable of detecting where the slope of a linear function changes and allows multiple linear models to be fitted to each distinct section of the time series (Toms and Lesperance 2003, Zeng *et al* 2019). For a time series y (SWS), a continuous PLRM with one TP can be described by equation (1):

$$y = \begin{cases} \beta_1 t + \varepsilon, & t \leq \mathrm{TP} \\ (\beta_1 + \beta_2)t - \beta_2 \mathrm{TP} + \varepsilon, & t \geqslant \mathrm{TP} \end{cases}, \quad (1)$$

where t is the year, β_1 and β_2 are regression coefficients, and ε is the residual. To avoid linear regression in a period with too few years, we confined the TP to be within the period 1981–2016. The trends before and after the TP were β_1 and $\beta_1 + \beta_2$, respectively. We used least-squares error techniques to fit the model to the data and determine a potential TP, β_1, and β_2. β_2 was calculated every year from 1981 to 2016. The necessity of introducing the TP was examined with the significance t-test under the null hypothesis that 'β_2 is not different from zero' (we assumed that there was one and only one TP). If the maximum of the absolute value for β_2 occurred in a given year, that year was determined to be the TP. Statistical significance for the regression included the goodness-of-fit, the P values for the entire model, and the trends before and after the TP.

The forward stepwise regression algorithm (FSRA) was employed to select the dominant CIs that had the largest explanatory power for the SWS changes. X_i (CIs) and Y (SWS) were selected to establish the regression model, as expressed by equation (2):

$$\begin{cases} Y = \alpha_i X_i + \delta, & i = 1, 2, \ldots, p \\ F^{(1)} = \max\left\{F_1^{(1)}, F_2^{(1)}, \ldots, F_p^{(1)}\right\}, \\ I = \{X_i | 1 < i < p\} \end{cases} \quad (2)$$

where α_i and δ are the regression coefficients and residual, respectively; $p = 17$; $F_i^{(1)}$ is the value of the F-test for α_i; and $F^{(1)}$ denotes the maximum value of $F_i^{(1)}$. Considering the threshold of significance level $\alpha = 0.01$, if $F^{(1)} \geqslant F_\alpha^{(1)}$, X_i is introduced into the model. I denotes the set of introduced X_i. When X_i is selected, the bivariate regression is estimated between Y and the subsets $\{X_i, X_1\}, \cdots, \{X_i, X_{i-1}\}, \{X_i, X_{i+1}\}, \cdots, \{X_i, X_p\}$ ($p - 1$ subsets). Similarly, the statistical value of the F-test is $F_{X_k}^{(2)} (X_k \neq I)$, and the maximum $F_{X_k}^{(2)}$ is then selected. If $F_{X_k}^{(2)} \geqslant F_\alpha^{(2)}$, X_k is input into the model. To avoid overfitting, the above steps are repeated six times, and, therefore, we validated the top six CIs for explaining SWS based on their statistical significance (Zeng *et al* 2019). Using the FSRA, a reconstructed wind speed (RWS) can be obtained based on the selected six CIs and their regression coefficients, as expressed in equation (3).

$$\mathrm{RWS} = \sum_{i=1}^{6} a_i X_i + b_0, \quad (3)$$

where a_i and b_0 are the regression coefficients and residual, respectively. To evaluate the importance of the selected CIs and examine the uncertainty of RWS, we randomly selected a 30% subset of the stations and performed the FSRA (repeated 300 times). The contribution of LOACs to the SWS tendency was estimated using equation (4):

$$Q = \frac{|T_R|}{|T_O|} \cdot 100\%, \quad (4)$$

where T_R and T_o denote the trends of the RWS and observations, respectively.

To estimate the trends for different wind categories and corresponding frequencies, light, gentle, moderate, and strong winds were defined as wind speeds <25th percentile, >25th percentile but <50th percentile, >50th percentile but <75th percentile, and >75th percentile, respectively. Correspondingly, the days with light, gentle, moderate, and strong winds were defined as the light, gentle, moderate, and strong windy days, respectively (Wang *et al* 2020). The periods 2021–2040, 2041–2060, and 2081–2100 represented the 'near-term,' 'mid-term,' and 'long-term' projections, respectively (Jiang *et al* 2020). The four seasons were defined as winter (December, January, and February), spring (March, April, and May), summer (June, July, and August), and autumn (September, October, and November).

3. Results

3.1. Robustness test of wind speed tendency

The temporal changes of SWS are shown in figure 1. The mean annual SWS decreased significantly from 1979 to 2011, at a rate of −0.108 m s^{-1} decade^{-1} ($P < 0.001$) (figure 1(a1)). A pronounced reduction was also discovered in seasonal SWSs, and all decreasing trends passed the significance t-test ($P < 0.001$) (table 1). Although the downward trends have been revealed and confirmed, the mean annual and seasonal SWSs have experienced increases in the recent decade (table 1). Therefore, a reversal of terrestrial stilling was observed in 2011, with the exception of summer (2009), with goodness-of-fit R^2 values of 82%, 48%, 69%, 71%, and 69% for annual mean, winter, spring, summer, and autumn, respectively. It is important to mention that the piecewise linear regression was determined via t-test significance, which could indicate a reversal of the trend in wind

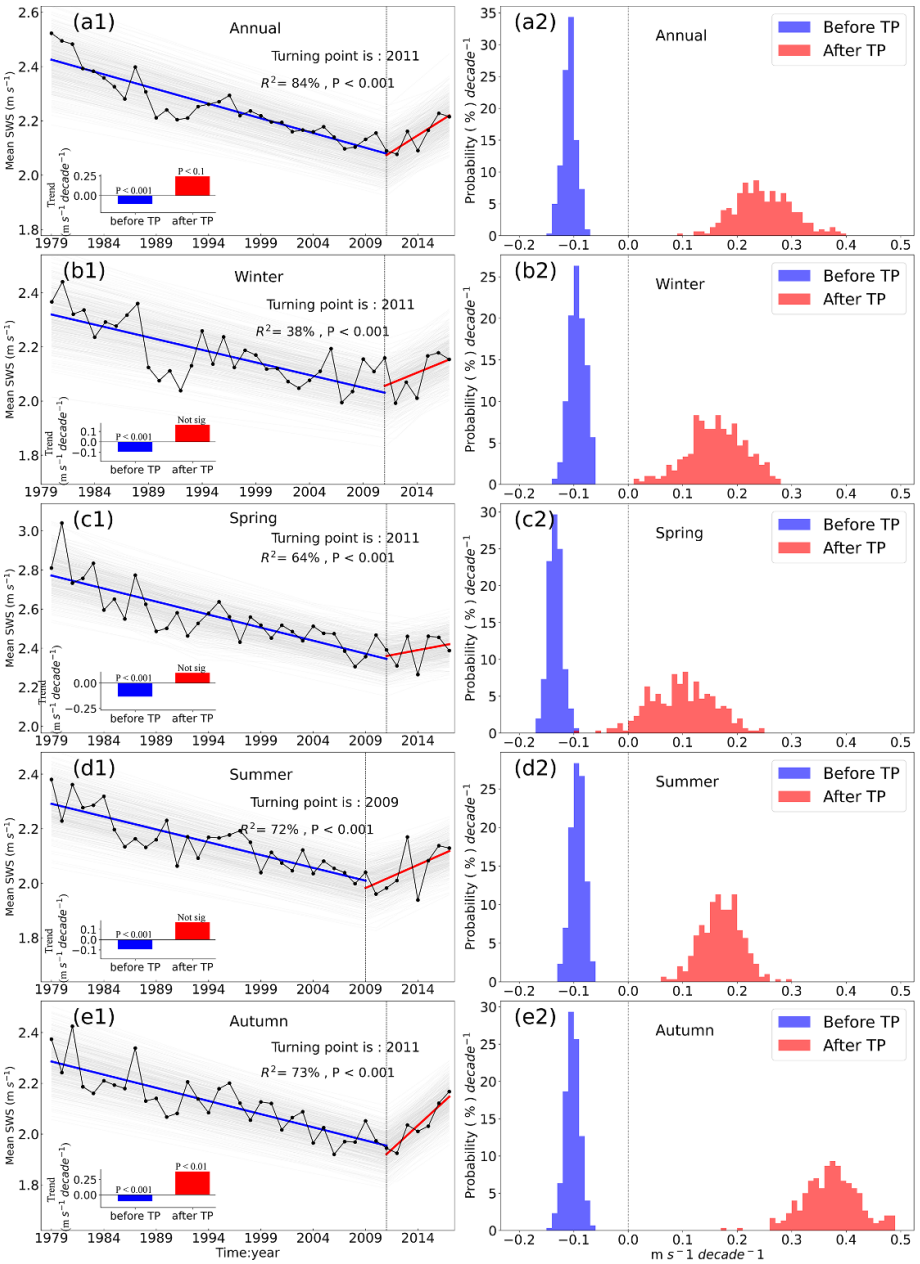

Figure 1. (a1)–(e1) Temporal changes of mean annual and seasonal SWSs from 1979 to 2017 (unit: m s^{-1}); (a2)–(e2) frequency distributions of the trends in mean annual and seasonal SWSs before and after the TPs identified in the 300 resampling results (unit: %). Each gray line ($n = 300$) is a piecewise linear fit for a randomly selected 30% subset of all stations. Blue and red lines are the piecewise linear fits. The trends during the two periods are presented in the inset. R^2 is the goodness-of-fit. The closer the R^2 is to 100%, the better the fitting effect. $P < 0.1$, 0.01, and 0.001 indicate the 90%, 99%, and 99.9% t-test confidence levels, respectively. Not sig indicates that the trend failed to pass the 90% significance t-test.

Table 1. Goodness-of-fit (R^2), TP, trend before and after TP (unit: m s^{-1} decade^{-1}), and relative frequency of the stations that exhibited negative and positive trends of SWS before and after TP for eastern China, 1979–2017. *, **, and *** denote the results passed the significance t-test at the 0.10, 0.01, and 0.001 levels, respectively.

			Before TP			After TP		
	R^2	TP	Trend	Negative	Negative significant $P < 0.10$	Trend	Positive	Positive significant $P < 0.10$
Annual	82%***	2011	0.108***	71.7%	55.63%	0.244*	53.5%	50.3%
Winter	48%***	2011	0.093***	67.9%	45.49%	0.162	54.0%	35.0%
Spring	69%***	2011	0.133***	74.6%	57.41%	0.101	45.2%	35.1%
Summer	71%***	2009	0.094***	66.9%	47.19%	0.169	61.2%	46.0%
Autumn	69%***	2011	0.104***	68.3%	49.06%	0.378**	65.1%	46.0%

speed change, although the trends after the TP could also be a flattening of the SWS decreasing trend.

To exclude the possibility that the TPs were caused by large SWS changes at only a few stations, we repeated the analyses 300 times by randomly resampling 30% of all the stations each time (gray lines in figure 1) to validate the TPs. The results revealed that the TPs in each subsample were close to the TPs in the total sample. The SWSs also mainly exhibited decreasing trends before the TP and increasing trends after. According to the estimates from the random resampling, the annual mean SWS changes before and after a specific TP were -0.108 ± 0.013 and 0.275 ± 0.054 m s^{-1} decade^{-1}, respectively (figure 1(a2)). Seasonally, the SWSs also showed downward trends before the TP during winter (–0.093 ± 0.014 m s^{-1} decade^{-1}), spring (–0.134 ± 0.014 m s^{-1} decade^{-1}), summer (–0.093 ± 0.013 m s^{-1} decade^{-1}), and autumn (–0.104 ± 0.014 m s^{-1} decade^{-1}), while the seasonal SWSs exhibited upward trends after the TP, at rates of 0.159 ± 0.054, 0.098 ± 0.057, 0.175 ± 0.039, and 0.377 ± 0.053 m s^{-1} decade^{-1}, respectively (figures 1(b2)–(e2)). A number of previous studies also discovered a reversal of stilling, e.g. all of China after the 1990s (Zhang and Wang 2020), southwestern China after 2000 (0.55 m s^{-1} decade^{-1}) (Yang *et al* 2012), and northwestern China from 1993 to 2005 (0.04 m s^{-1} decade^{-1}) (Li *et al* 2018b). The magnitudes and TPs of the SWS reversal were inconsistent, however, due to the differences in study regions, periods, datasets, and methods. Although some former studies also found the SWS reversal in recent decades at regional scales, the TPs were not examined.

Spatial patterns of the SWS trends before and after the TPs were revealed (figure 2), and the results show that 71.7%, 67.9%, 74.6%, 66.9%, and 68.3% of the total stations exhibited mean annual, winter, spring, summer, and autumn SWSs with decreasing trends before the TP, respectively. Conversely, after the TP, 53.5%, 54.0%, 45.2%, 61.2%, and 65.1% of the total stations exhibited mean annual, winter, spring, summer, and autumn SWSs with increasing trends, respectively (table 1). Hence, SWS reversal did not mean that all stations displayed increasing SWSs. Furthermore, the annual and seasonal distributions of the TPs for all stations showed that most TPs occurred around 2011 (figure S2).

3.2. Trends for different categories of wind speeds and windy days

Given that the decrease or increase in SWS could be due to different wind categories, the trends for light, gentle, moderate, and strong winds before and after the TP were investigated. The annual trend for all wind categories was decreasing before the TP and increasing after (figures 3(a1)–(e1)). Before the TP, all trends passed the significance *t*-test at the 0.001 level; the most significant reduction was found in strong winds, at rates of −0.17, −0.14, −0.09, −0.12, and −0.15 m s^{-1} decade^{-1} in mean annual, winter, spring, summer, and autumn, respectively (figures 3(a1)–(e1)). After the TP, all wind categories displayed increasing trends, with the weakest increase observed in strong winds during autumn (0.18 m s^{-1} decade^{-1}) (figure 3(e1)), and the most significant increase observed in strong winds during winter (0.33 m s^{-1} decade^{-1}) (figure 3(b1)). The trend differences among different wind categories in the same season were not pronounced either before or after the TP. Before the TP, the maximum and minimum trend differences were observed in annual mean and spring, with standard deviations of 0.10 and 0.025 m s^{-1} decade^{-1}, respectively, while after TP the maximum and minimum trend differences occurred in winter and spring, with standard deviations of 0.13 and 0.046 m s^{-1} decade^{-1}, respectively (figure 3(c1)).

The frequency trends for different windy days were investigated (figures 3(a2)–(e2)). The decrease in annual mean SWS before the TP was caused by the decrease in the frequency of strong winds (–47.30 d decade^{-1}, $P < 0.001$), while the increase in annual mean SWS after the TP was due to the increase in the frequency of moderate winds (46.00 d decade^{-1}, $P < 0.10$) and strong winds (153.71 d decade^{-1}, $P < 0.10$) (figure 3(a2)). The seasonal decreasing and increasing trends in SWSs before and after the TPs were attributed to the decrease and increase in days with strong winds. During winter, spring, summer, and autumn, the decreasing trends before the TP were −7.49, −13.41, −13.76, and −11.23 d decade^{-1}, respectively, and the increasing trends after the TP were 44.57, 15.43, 33.71, and 56.00 d decade^{-1}, respectively (figures 3(b2)–(e2)). Meanwhile, all downward trends passed the significance *t*-test at the 0.001 level. The reduction and increase in SWS before and after the TP were also accompanied by corresponding increases and decreases in the frequencies of light and gentle winds. Consequently, SWS changes mainly displayed two features before and after the TP: (a) all wind categories exhibited decreasing trends before the TP, and increasing trends after; and (b) the downward trends in SWSs before the TP mainly manifested as the decrease in the frequency of strong windy days and the increase in the frequency of light windy days, and the upward trends after the TP mainly manifested as the increase in the frequency of strong windy days and the decrease in the frequency of light windy days.

3.3. Potential effects of LOACs on long-term SWS changes

Wind is physically created by pressure gradients, which are due to the uneven heating of the Earth's surface, and the uneven heating is to a large extent described by CIs for LOACs (Zeng *et al* 2019). Hence,

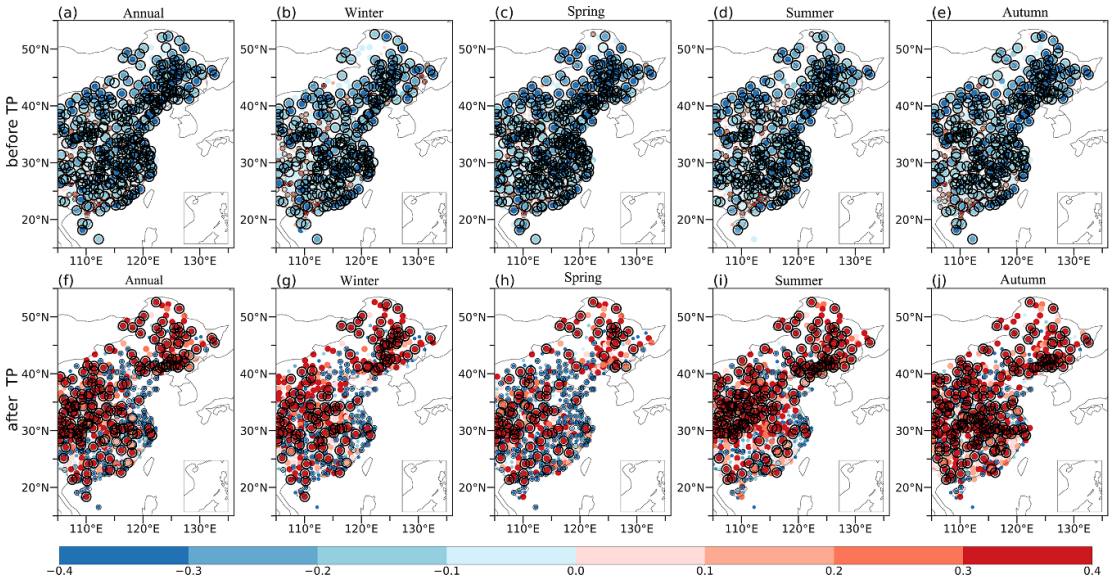

Figure 2. Spatial patterns of linear trends during the two periods (a)–(e) 1979–TP and (f)–(j) TP–2017 (unit: m s^{-1} $decade^{-1}$): (a) and (f) annual mean; (b) and (g) winter; (c) and (h) spring; (d) and (i) summer; (e) and (j) autumn. Circles indicate that the trends passed the significance *t*-test at the 0.10 level.

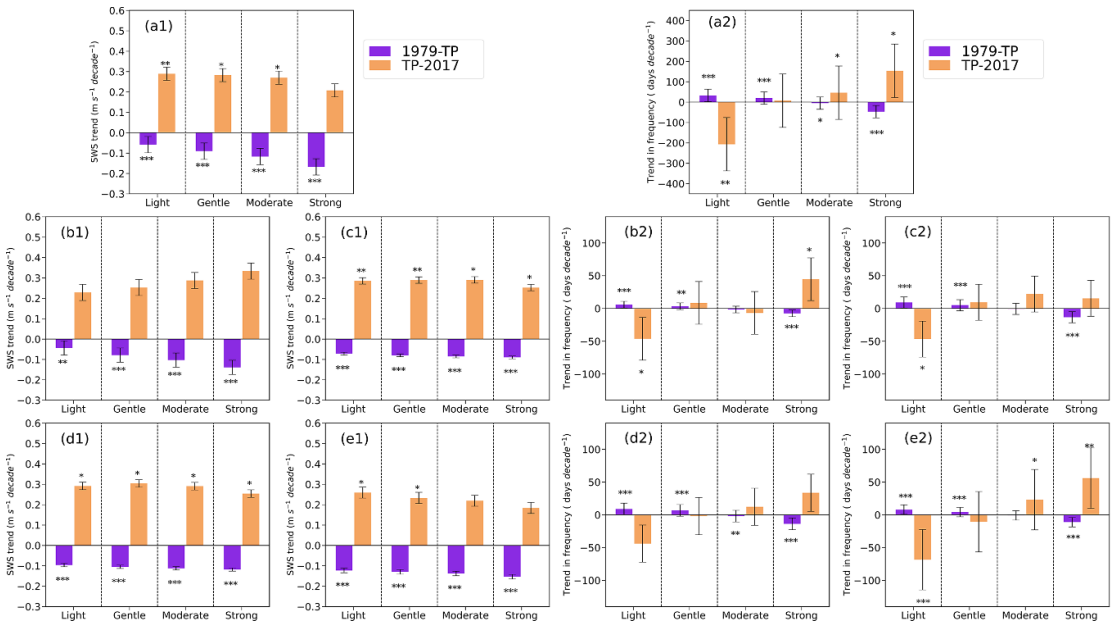

Figure 3. Linear trends of different wind categories (light, gentle, moderate, and strong) (unit: m s^{-1} $decade^{-1}$), and linear trends of annual and seasonal frequencies of different wind categories (unit: days $decade^{-1}$) for 1979–TP and TP–2017, respectively. 1 and 2 denote the linear trends of speeds and frequencies, respectively. (a)–(e) denote annual mean, winter, spring, summer, and autumn, respectively. The significances of the trends are as follows: *, **, and *** denote the trends passing the significance *t*-test at the 0.10, 0.01, and 0.001 levels, respectively. Blank indicates a trend is not significant. Black bars denote the uncertainties of the estimation results.

the LOACs are important to SWS changes. In this section, we will investigate whether decadal-scale LOACs can explain the SWS changes over China. We found that no single climate index had large explanatory power, but together the CIs generated a large amount of explanatory power. Nevertheless, the fit improvement also became marginal when the number of CIs retrained in the stepwise regression was larger (e.g. the explanatory power changed by only 6% from 6 CIs to 12 CIs) (figure 4(a)). The PDO exhibited the largest explanatory power in annual terms, followed in decreasing order by the WHWP, WPI, AO, Solar, and Niño 3. The total explanatory power for the selected CIs was 86.0%. Seasonally, the importance levels of CIs for the SWSs were not consistent, with the exception of the PDO. These results imply that the SWS changes during different seasons could be influenced by different LOACs, although

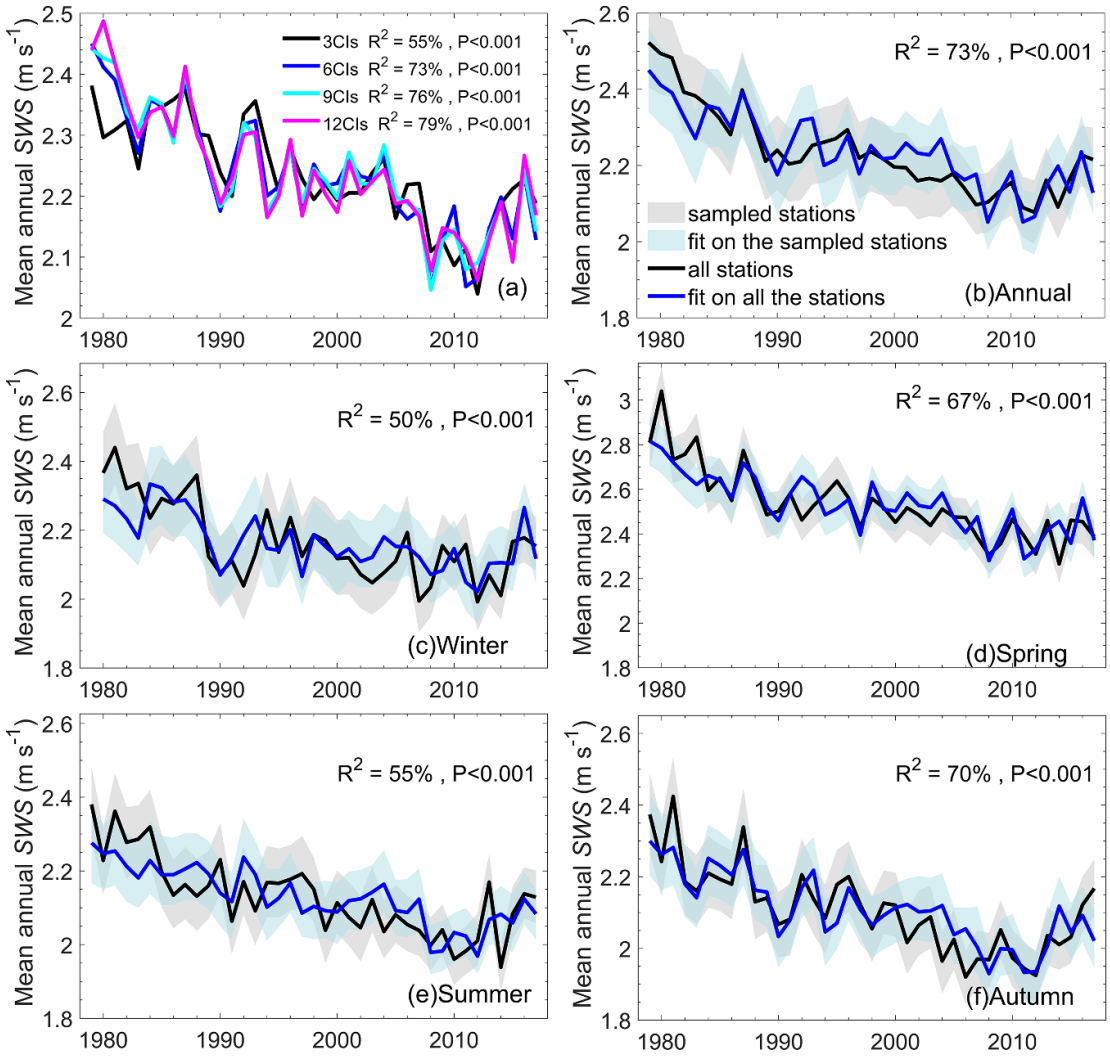

Figure 4. (a) Temporal changes of RWSs with different CIs based on a stepwise forwarding regression algorithm; (b)–(f) temporal changes of observed wind speeds (black lines) and RWSs (blue lines). Uncertainties of results are indicated by the shading based on a randomly selected 30% subset of the stations (repeated 300 times). Inset black numbers are the correlation coefficients between observed wind speeds and RWSs. (a)–(e) denote annual mean, winter, spring, summer, and autumn, respectively.

the effect of the PDO on SWS was evident in all four seasons. The total explanatory power values of the selected CIs reached 71%, 82%, 74%, and 84% in winter, spring, summer, and autumn, respectively (table 2). To determine if these CIs could be selected in most cases, we carried out the 300-repetition test (30% of the stations were chosen at random for each test). The results revealed that the CIs could be selected in most cases, especially for the CIs ranked 1 and 2. Meanwhile, the selected numbers decreased in the 300-repetition simulations accompanied by the delay of the CIs entering the model.

Based on the FSRA, the RWSs matched the observations well from 1979 to 2017, implying that the RWSs were capable of reproducing the observation changes. The correlations between the RWSs and observations were 0.86 ($P < 0.001$), 0.71 ($P < 0.001$), 0.80 ($P < 0.001$), 0.73 ($P < 0.001$), and 0.84 ($P < 0.001$) for mean annual, winter, spring, summer, and autumn, respectively (figures 4(b) and (f)). The detrended RWSs and observations were analyzed, and the results also showed that both the RWSs and observations displayed synchronous variability after detrending. The goodness-of-fit between the detrended RWSs and observations reached 0.75 ($P < 0.001$), 0.69 ($P < 0.001$), 0.77 ($P < 0.001$), 0.54 ($P < 0.001$), and 0.66 ($P < 0.001$) in annual mean, winter, spring, summer, and autumn, respectively (figure S3). Hence, the effect of LOACs on the SWS variations was significant. We also investigated whether the selected CIs displayed the TPs in 2011, finding that some did, although the fitted equations of most CIs were not significant (table S2). Consequently, we concluded that SWS changes cannot be simply linked with just one ocean-atmosphere oscillation index, but should be determined by the combined effects of variations in multiple LOACs.

Since the RWSs can capture the temporal changes of the observed SWSs, the contributions of LOACs to the tendencies of SWSs can be estimated. Both the

Table 2. The six selected CIs based on the FSRA during the common period with SWS from 1979 to 2017. The number of the first column denotes the order of the CIs entering the model (1 and 6 are the first and last CIs chosen, respectively). The earlier the CIs enter the model, the larger the explanatory power of the predictor. Numbers in parentheses denote the selected numbers of CIs in the 300-repetition test (30% of the stations were chosen at random for each test). Explanatory power refers to the total variation of the model explaining the annual SWS and the SWS for each of the four seasons.

Number	Annual	Winter	Spring	Summer	Autumn
1	PDO (300)	PDO (299)	PDO (295)	PDO (300)	PDO (300)
2	WHWP (300)	WHWP (296)	Solar (300)	WHWP (298)	WHWP (298)
3	WPI (299)	AO (174)	AO (300)	WPI (266)	WPI (281)
4	AO (297)	WPI (297)	WHWP (298)	AMM (266)	AO (288)
5	Solar (293)	WPSHA (167)	WPI (298)	Solar (219)	Solar (284)
6	Niño 3 (122)	EAWM (167)	Niño 3 (237)	Niño 3 (221)	Niño 4 (126)
Explanatory power (R)	86%	71%	82%	74%	84%

RWSs and observations exhibited decreasing trends in all four seasons. The largest trend difference was found in spring (0.040 m s^{-1} $decade^{-1}$), and the smallest in autumn (0.019 m s^{-1} $decade^{-1}$) (figure 5(a)). The reductions in observed SWSs can be impacted by LOACs (Zeng *et al* 2019), urbanization (Li *et al* 2018a), aerosols (Bichet *et al* 2012), greenhouse gases (GHGs) (Zha *et al* 2020), and other factors, although the RWSs only include the LOACs effects. Accordingly, the reductions of the RWSs were slower than those of the observations. The contribution of LOACs to the downward trend of SWS was >70.0%; thus, the total contribution of other factors was <30.0%. The largest contribution was found in autumn (82.75%), and the smallest in winter (70.30%). After the TP, both the RWSs and observations exhibited increasing trends in all four seasons, with the RWS trends weaker than those of the observations (figure 5(b)). The contribution of LOACs to the upward trend of SWS was >60.0% in all seasons but autumn. The largest contribution was found in spring (91.02%), and the smallest in autumn (41.01%). These results indicate that the SWS slowdown before the TP and the increase after can mainly be attributed to the variations of LOACs.

3.4. Future changes in SWS

The above results demonstrate that the SWS reversal in the recent decades is an established phenomenon. In this section, we investigate whether the SWS strengthening will continue in the future. First, the performance of the CMIP6 models in simulating the historical SWS over eastern China was evaluated (table S3). Significant positive correlations were found in six of the 23 models, with the largest correlation in the EC-Earth3 (0.63). The wind speed difference (WSD) between the CMIP6 and observations exhibited positive values in all models, with a mean bias of 1.22 $\pm$ 0.58 m s^{-1}. The WSD between the EC-Earth3 and observations was 1.24 m s^{-1}, which was close to the mean bias of all models. Of the 23 models, the strongest weakening was found in the EC-Earth3 (–0.044 m s^{-1} $decade^{-1}$). A comparison of the correlation coefficient, WSD, and trends of the EC-Earth3 with those of the other models revealed that the EC-Earth3 simulation of the SWS changes exhibited better performance. Accordingly, the EC-Earth3 was selected to project the SWS changes. The EC-Earth3 has been extensively used in many fields and has been demonstrated to be capable of capturing the correct patterns of LOACs (Doblas-Reyes *et al* 2017, Han *et al* 2020, Ringgaard *et al* 2020, Wyser *et al* 2020). Most CMIP6 models cannot satisfactorily assimilate significant reductions in SWS (table S3), possibly because changes in surface roughness are not included in the surface boundary conditions of the models, or perhaps due to missing model physics, inappropriate model resolution, or inaccuracy of atmospheric boundary layer processes implemented in the data assimilation systems (Chen *et al* 2012, Zeng *et al* 2019). Hence, more efforts are required to improve surface process parameterization schemes and their connections to LOACs in climate models and operational weather data assimilation systems (Zeng *et al* 2019).

The SWS is predicted to exhibit a decreasing trend in the future (2021–2100), with the downward trend in the SSP585 scenario being stronger than that of either the SSP245 or SSP370 (figure 6(a)). For the near-term, mid-term, and long-term periods, the SWS only showed an increase in the near-term under the SSP245. Comparing the near-term and mid-term predictions with the long-term, a stronger SWS reduction was found in the long-term. Consequently, the reversal is only expected to last for a short period before winds start decreasing again. Moreover, enhanced decreasing trends were associated with stronger emission scenarios, with the most pronounced decreasing trend found in the SSP585 (figure 6(b)). Similar results have also been reported in previous studies. For instance, Li *et al* (2020) found that the wind speed may decrease over East Asia. Jiang *et al* (2018) predicted that the wind speeds during the 21st century will decrease slightly in China. Gao *et al* (2019) discovered that the wind resources in most parts of China exhibited slight decreases under the

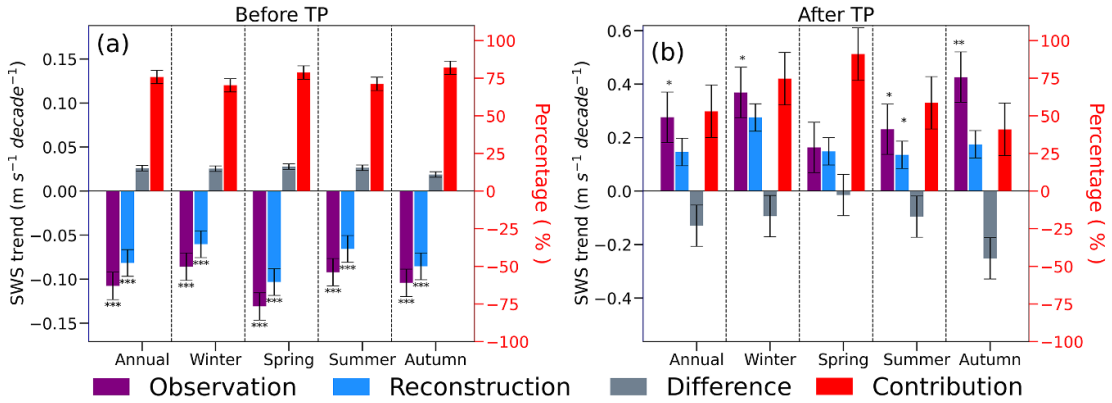

Figure 5. Linear trends of observations and RWSs (unit: m s^{-1} decade^{-1}), and their differences, as well as the relative contributions of LOACs (unit: %) to the long-term changes in SWSs before and after the TP. (a) and (b) denote the periods before and after the TP, respectively. The significances of the trends are as follows: *, **, and *** denote the trends passing the significance *t*-test at the 0.10, 0.01, and 0.001 levels, respectively. Blank indicates a trend is not significant. Black bars denote the uncertainty ranges of the estimation results. Difference denotes the trend difference between RWSs and observations (RWSs minus observations).

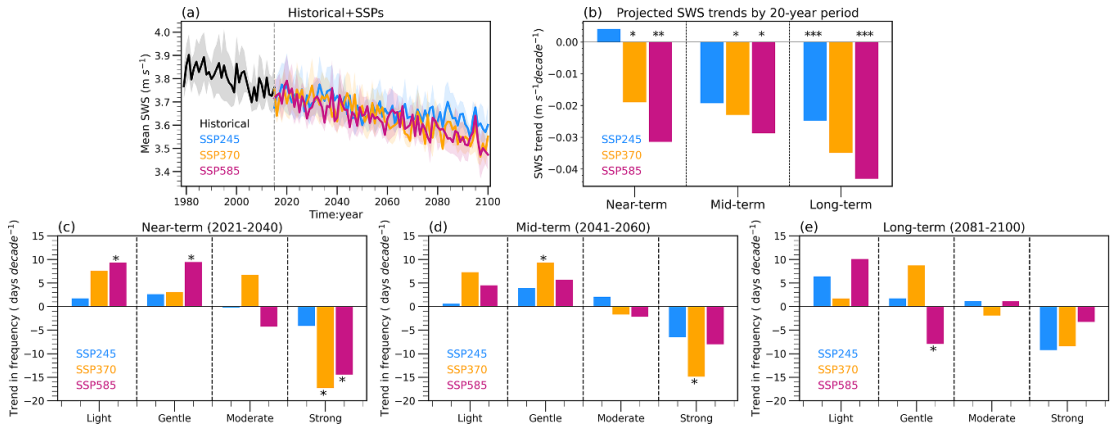

Figure 6. (a) Temporal changes of mean annual SWS over eastern China from 1979 to 2100 (unit: m s^{-1}). Historical (black), SSP245 (light blue), SSP370 (yellow), and SSP585 (red) simulations by the EC-Earth3 model are shown for the 25th and 75th percentiles (shading). (b) Projected trends of SWSs for near-term (2021–2040), mid-term (2041–2060), and long-term (2081–2100) under the SSP245 (light blue), SSP370 (yellow), and SSP585 (red) scenarios (unit: m s^{-1} decade^{-1}). (c) Projected trends in frequencies of different wind categories for the near-term projection (unit: d decade^{-1}). Light blue, yellow, and red bars denote the SSP245, SSP370, and SSP585 scenarios, respectively. (d) and (e) are the same as (c), but for mid-term and long-term projections, respectively. *, **, and *** denote the trends passing the significance *t*-test at the 0.10, 0.01, and 0.001 levels, respectively. Blank indicates a trend is not significant.

RCP4.5 and RCP8.5 scenarios. Research estimating the changes of different wind categories in the future remain insufficient, however.

Given that the future changes of SWS could be caused by the changes of different wind categories, the frequency trends for different types of windy days were determined. For the near-term projections (figure 6(c)), under the SSP245, SSP370, and SSP585 scenarios, the frequency of light winds increased, at rates of 1.7, 7.5, and 9.3 d decade^{-1}, respectively, and the gentle winds increased at rates of 2.6, 3.1, and 9.4 d decade^{-1}, respectively, although the strong winds decreased, at rates of −4.1, −17.3, and −14.5 d decade^{-1}. Accordingly, as emissions increased, days with light and gentle winds increased while days with strong winds decreased. The decreasing trend of days with strong winds in the SSP245 was weaker than the trends in the SSP370 and SSP585; hence, compared to the SSP370 and SSP585, a weak SWS recovery was found in the SSP245. For the mid-term and long-term projections, the reductions in annual mean SWSs were induced by the decreases of the days with strong winds in all SSPs.

4. Discussion

Seasonal SWSs manifesting different trends were also reported in prior studies (You *et al* 2010, Lin *et al* 2013, Hu *et al* 2019). Winter SWS decline was associated with global-scale warming that may be attributed to increased greenhouse gas emissions, and the summer SWS decline was associated with local cooling over south-central China that may be the result of air pollution (Xu *et al* 2006). Spring SWS over

northern China could be affected by the winter sea surface temperatures over the North Atlantic and North Pacific Oceans (Hu *et al* 2019), and autumn SWS changes may be related to the AO (Zhang *et al* 2020). We theorized that the different trends exhibited by the seasonal SWSs could be due to the effects of LOACs (Wu *et al* 2018a, 2018b). Accordingly, we assessed the effects of LOACs on the SWSs. We propose that the SWS changes cannot be simply linked with just one index but could be determined by the combined effects of variations in multiple LOACs.

There are some theories regarding the mechanisms behind the effects of LOACs changes on regional SWSs. With respect to the PDO, the temperature gradient during its negative phase generates an easterly component of surface wind, which weakens the prevailing westerly winds in the mid-latitudes (Zeng *et al* 2019). As for the AO, the stronger it becomes, the more the Ferrell cell is enhanced at high latitudes, which induces meridional flow anomalies. The anomalous meridional flows transport heat from lower latitudes to higher latitudes, thereby reducing the north-south temperature difference, which in turn decreases surface winds (Li and Wang 2003). The Western Pacific (WP) teleconnection is a meridional dipole pattern of atmospheric circulation anomalies at middle and high latitudes of the North Pacific, which significantly affect the intensity and position of the Aleutian low (Park and Ahn 2015). The variability in SWS is significantly correlated with the intensity of the Aleutian low (Zhang and Wang 2020); therefore, it is possible that the WP pattern primarily alters SWS by affecting the intensity and position of the Aleutian low. The intensity, shape, and location of the WPSHA dominate the large-scale quasi-stationary frontal zones in East Asia (Wang *et al* 2001), although the influences of the WPSHA, WHWP, AMM, Solar, and Niño indices on SWS have yet to be reported. Since the interaction and modulation among different LOACs are considerable, it is difficult to isolate and quantify the contributions of different LOACs to SWS changes and reveal the corresponding mechanisms.

Additionally, some anthropogenic activities, such as urbanization (Li *et al* 2018a), GHGs (Zhang *et al* 2016), anthropogenic aerosols (Li *et al* 2016), and anthropogenic heat release (Zhang *et al* 2015), can alter LOACs. The ways in which these anthropogenic factors influence LOACs, which then affect SWS changes, have not yet been determined. These aspects may be further examined and identified using detailed modeling studies.

5. Conclusions

The recently observed SWS reversal was determined to be an established phenomenon, with rates of 0.244, 0.162, 0.101, 0.169, and 0.378 m s^{-1} $decade^{-1}$ for mean annual, winter, spring, summer, and autumn, respectively. The decrease of mean annual SWS before the TP was induced by the decrease in the frequency of strong windy days, at the rate of −47.30 d $decade^{-1}$, while the increase after the TP was due to the increase in the frequency of moderate and strong windy days, at rates of 46.00 and 153.71 d $decade^{-1}$, respectively, as well as the decrease in the frequency of light windy days, at the rate of −206.86 d $decade^{-1}$.

The RWSs matched well with the observations during the period 1979–2017. The correlations between the observations and RWSs were 0.856, 0.710, 0.796, 0.733, and 0.835 for annual mean, winter, spring, summer, and autumn, respectively. The SWS changes cannot simply be related to one ocean-atmosphere oscillation but must be linked to the combined effects of variations in multiple LOACs. The contributions of LOACs to the decreasing trends of SWSs before the TP were >70.0%, and the contributions of LOACs to the increasing trends of SWSs after the TP were >60.0%, with the exception of autumn. Therefore, the SWS slowdown before the TP and increase after the TP were mainly attributed to the variations of LOACs.

During the historical period (1979–2014), the majority of the CMIP6 models did not reproduce the significantly decreasing trend of SWS. Of the 23 models evaluated, the EC-Earth3 produced the best simulation results for the SWS over eastern China. The results revealed that the correlation coefficient between the EC-Earth3 and observations reached 0.63, the WSD between the EC-Earth3 and observations was 1.24 m s^{-1}, and the greatest weakening was produced by the EC-Earth3 (–0.044 m s^{-1} $decade^{-1}$). Based on the EC-Earth3, the SWS only exhibited increases in the near-term under the SSP245 scenario. For the mid-term and long-term forecasts, the reduction in mean annual SWS grew more pronounced as the emissions strengthened, a trend that was induced by the decrease in days with strong winds.

Data availability statement

The data that support the findings of this study are openly available at the following URL/DOI: http://data.cma.cn/data/cdcdetail/dataCode/SURF_CLI_CHN_MUL_DAY_V3.0.html.

Acknowledgments

The work is supported by National Key Research and Development Program of China (2016YFA0600403, 2018YFA0606004), Natural Science Foundation of China (42005023, 41675149, 41775087, 41875178, 41865001), Project funded by China Postdoctoral Science Foundation (2019M660761), and Jiangsu Province Project (BK20181099; BRA2020429). This work is also supported by the Program for Key Laboratory in University of Yunnan Province and

the Program for Special Research Assistant Project of Chinese Academy of Sciences.

ORCID iDs

Cheng Shen https://orcid.org/0000-0003-1727-2638
Deming Zhao https://orcid.org/0000-0003-0063-9376
Wenxuan Fan https://orcid.org/0000-0003-2457-5821

References

Azorin-Molina C S, Vicente-Serrano M, McVicar T R, Jerez S, Sanchez-Lorenzo A, Lopez-Moreno J L, Revuelto J, Trigo R M, Lopez-Bustins J A and Espirito-Santo F 2014 Homogenization and assessment of observed near-surface wind speed trends over Spain and Portugal, 1961–2011 *J. Clim.* **27** 3692–712

Barnston A G and Livezey R E 1987 Classification, seasonality and persistence of low-frequency atmospheric circulation patterns *Mon. Weather Rev.* **115** 1083–126

Bichet A, Wild W, Folini D and Schar S 2012 Causes foe decadal variations of speed over land: sensitivity studies with a global climate model *Geophys. Res. Lett.* **39** L11701

Chen L, Li D and Pryor S C 2013 Wind speed trends over China: quantifying the magnitude and assessing causality *Int. J. Climatol.* **33** 2579–90

Chen L, Pryor S C and Li D L 2012 Assessing the performance of intergovernmental panel on climate change AR5 climate models in simulating and projecting wind speeds over China *J. Geophys. Res. Atmos.* **117** D24102

Chiang J C H and Vimont D J 2004 Analogous meridional modes of atmospheric-ocean variability in the tropical Pacific and tropical Atlantic *J. Clim.* **17** 4143–58

China Meteorological Administration (CMA) 2003 *Ground Surface Meteorological Observation* (Beijing: China Meteorological Press) p P157

Cook B I, Mankin J S, Marvel K, William A P, Smerdon J E and Anchukaitis K J 2020 Twenty-first century drought projections in the CMIP6 forcing scenarios *Earth's Future* **8** e2019EF001461

Dadaser-Celik F and Cengiz E 2014 Wind speed trends over Turkey from 1975–2006 *Int. J. Climatol.* **34** 1913–27

Doblas-Reyes F J *et al* 2017 Using EC-Earth for climate prediction research *ECMWF Newsl.* **154** 35–40

Enfield D B, Mestas-Nunez A M, Mayer D A and Cid-Serrano L 1999 How ubiquitous is the dipole relationship in tropical Atlantic sea surface temperature? *J. Geophys. Res. Oceans* **104** 7841–8

Eyring V, Bony S, Meehl G A, Senior C A, Stevens B, Stouffer R J and Taylor K E 2016 Overview of the Coupled Model Intercomparison Project Phase 6 (CMIP6) experimental design and organization *Geosci. Model Dev.* **9** 1937–58

Fan X W, Duan Q Y, Shen C W, Wu Y and Xing C 2020 Global surface air temperature in CMIP6: historical performance and future changes *Environ. Res. Lett.* **15** 104056

Gao Y, Ma S X and Wang T 2019 The impact of climate change on wind power abundance and variability in China *Energy* **189** 116215

Gilliland J M and Keim B D 2018 Surface wind speed: trend and climatology of Brazil from 1980–2014 *Int. J. Climatol.* **38** 1060–73

Guo H, Xu M and Hu Q 2011 Changes in near-surface wind speed in China: 1969–2005 *Int. J. Climatol.* **31** 349–58

Han Z X, Zhang Q, Wen Q, Lu Z Y, Feng G L, Su T and Zhang Q 2020 The changes in ENSO-induced tropical Pacific precipitation variability in the past warm and cold climates from the EC-Earth simulation *Clim. Dyn.* **55** 503–19

He Y P, Monahan A H, Jones C G, Dai A G, Biner S, Caya D and Winger K 2010 Probability distributions of land surface wind speeds over North America *J. Geophys. Res. Atmos.* **115** D04103

Higgins R W, Leetmaa A and Kouskv V E 2002 Relationships between climate variability and winter temperature extremes in the United States *J. Clim.* **15** 1555–72

Hu Y H, Gong D Y, Mao R and Shi X X 2019 Relationships between interannual variations of spring winds in the agr0-pastoral transitional zone of Northern China winter sea surface temperature *Prog. Geogr.* **38** 709–17 (in Chinese)

Huang Y, Wang B, Li X and Wang H 2018 Changes in the influence of the western Pacific subtropical high on Asian summer monsoon rainfall in the late 1900s *Clim. Dyn.* **51** 443–55

Jiang J, Zhou T J, Chen X L and Zhang L X 2020 Future changes in precipitation over Central Asia based on CMIP6 projections *Environ. Res. Lett.* **15** 054009

Jiang Y, Luo Y, Zhao Z C and Tao S W 2010 Changes in wind speed over China during 1956–2004 *Theor. Appl. Climatol.* **99** 421–30

Jiang Y, Xu X Y, Liu H W, Wang W B and Dong X G 2018 Projection of surface wind by CMIP5 and CMIP3 in China in the 21st century *J. Meteorol. Environ.* **34** 56–63

Kim J C and Paik K 2015 Recent recovery of surface wind speed after decadal decrease: a focus on South Korea *Clim. Dyn.* **45** 1699–712

Li D, Feng J L, Dosio A, Qi J F, Xu Z H and Yin B H 2020 Historical evaluation and future projections of 100-m wind energy potentials over CORDEX-East Asia *J. Geophys. Res. Atmos.* **125** e2020JD032874

Li J P and Wang J X L 2003 A modified zonal index and its physical sense *Geophys. Res. Lett.* **30** 1632

Li J P and Zeng Q C 2002 A unified monsoon index *Geophys. Res. Lett.* **29** 1274

Li J P and Zeng Q C 2003 A new monsoon index and the geographical distribution of the global monsoons *Adv. Atmos. Sci.* **20** 299–302

Li Y P, Chen Y N, Li Z and Fang G H 2018b Recent recovery of surface wind speed in northwest China *Int. J. Climatol.* **38** 4445–58

Li Z Q *et al* 2016 Aerosol and monsoon climate interactions over Asia *Rev. Geophys.* **54** 866–929

Li Z Q, Song L L, Ma H, Xiao J J, Wang K and Chen L 2018a Observed surface wind speed declining induced by urbanization in East China *Clim. Dyn.* **50** 735–49

Lin C G, Yang K, Qin J and Hu Y 2013 Observation coherent trends of surface and upper-air wind speed over China since 1960 *J. Clim.* **26** 2891–903

Mantua N J, Hare S R, Zhang Y, Wallace J M and Francis S C 1997 A Pacific interdecadal climate oscillation with impacts on salmon production *Bull. Am. Meteorol. Soc.* **78** 1069–80

McMahon T A, Peel M C, Lowe L, Srikanthan R and McVicar T R 2013 Estimating actual, potential, reference crop and pan evaporation using standard meteorological data: a pragmatic synthesis *Hydrol. Earth Syst. Sci.* **17** 1331–63

McVicar T R *et al* 2012 Global review and synthesis of trends in observed terrestrial near-surface wind speeds: implications for evaporation *J. Hydrol.* **24** 182–205

Moen J and Brekke A 1993 The solar flux influence on quiet time condutances in the auroral ionosphere *Geophys. Res. Lett.* **20** 971–4

Naizghi M S and Ouarda T B 2017 Teleconnections and analysis of long-term wind speed variability in the UAE *Int. J. Climatol.* **37** 230–48

Nan S L and Li J P 2003 The relationship between summer precipitation in the Yangtze River valley and the previous Southern Hemisphere Annular Mode *Geophys. Res. Lett.* **30** 2266

Nchaba T, Mpholo M and Lennard C 2017 Long-term austral summer wind speed trends over southern Africa *Int. J. Climatol.* **37** 2850–62

O'Neill B C *et al* 2017 The roads ahead: narratives for shared socioeconomic pathways describing world futures in the 21st century *Glob. Environ. Change* **42** 169–80

Park H J and Ahn J B 2015 Combined effect of the Arctic oscillation and the Western Pacific pattern on East Asia winter temperature *Clim. Dyn.* **46** 3205–21

Ringgaard I M, Yang S T, Kaas E and Christensen J H 2020 Barents-Kara sea ice and European winters in EC-Earth *Clim. Dyn.* **54** 3323–38

Roderick M L, Rotstayn L D, Farquhar G D and Hobbins M T 2007 On the attribution of changing pan evaporation *Geophys. Res. Lett.* **34** L17403

Toms J D and Lesperance M L 2003 Piecewise regression: a tool for identifying ecological thresholds *Ecology* **84** 2034–41

Trenberth K E and Stepaniak D P 2001 Indices of El Niño evolution *J. Clim.* **14** 1697–701

Vautard R, Cattiaux J L, Yiou P, Thepaut J N and Ciais P 2010 Northern Hemisphere atmospheric stilling partly attributed to an increase in surface roughness *Nat. Geosci.* **3** 756–61

Wang C and Enfield D B 2001 The tropical Western Hemisphere warm pool *Geophys. Res. Lett.* **28** 1635–8

Wang J, Feng J M, Yan Z W, Qiu Y and Cao L J 2020 An analysis of the urbanization contribution to observed terrestrial stilling in the Beijing-Tianjin-Hebei region of China *Environ. Res. Lett.* **15** 032062

Wang L 2014 An intensity index for the East Asian winter monsoon *J. Clim.* **27** 2361–74

Wang M R, Wang J, Chen D L, Duan A M, Liu Y M, Zhou S W, Guo D, Wang H M and Ju W M 2019 Recent recovery of the boreal spring sensible heating over the Tibetan Plateau will continue in CMIP6 future projections *Environ. Res. Lett.* **14** 124066

Wu J, Zha J L and Zhao D M 2016 Estimating the impact of the changes in land use and cover on the surface wind speed over the East China Plain during the period 1980–2011 *Clim. Dyn.* **46** 847–63

Wu J, Zha J L and Zhao D M 2017 Evaluating the effects of land use and cover change on the decrease of surface wind speed over China *Clim. Dyn.* **48** 131–49

Wu J, Zha J L, Zhao D M and Yang Q D 2018a Changes of wind speed at different heights over China during 1980–2011 *Int. J. Climatol.* **38** 4476–95

Wu J, Zha J L, Zhao D M and Yang Q D 2018b Changes in terrestrial near-surface wind speed and their possible causes: an overview *Clim. Dyn.* **51** 2039–78

Wyser K, Noije T, Yang S, Hardenberg J, Donnell D and Doscher R 2020 On the increased climate sensitivity in the EC-Earth model from CMIP5 to CMIP6 *Geosci. Model Dev.* **13** 3465–74

Xu M, Chang C P, Fu C B, Qi Y, Robock A, Robinson D and Zhang H M 2006 Steady decline of East Asian monsoon winds, 1969–2000: evidence from direct ground measurements of wind speed *J. Geophys. Res.* **111** D24111

Yang X M, Li Z X, Feng Q, He Y Q, An W L, Zhang W, Cao W H, Yu T F, Wang Y M and Wilfred H T 2012 The decreasing wind speed in southwestern China during 1969–2009, and possible causes *Quat. Int.* **263** 71–84

You Q L, Kang S C, Flugel W A, Pepin N, Yan Y P and Huang J 2010 Decreasing wind speed and weakening latitudinal surface pressure gradients in the Tibetan Plateau *Clim. Res.* **42** 57–64

Zeng Z Z *et al* 2019 A reversal in global terrestrial stilling and its implications for wind energy production *Nat. Clim. Change* **9** 979–85

Zha J L, Wu J and Zhao D M 2016 Changes of probabilities in different wind grades induced by land use and cover change in Eastern China Plain during 1980–2011 *Atmos. Sci. Lett.* **17** 264–9

Zha J L, Wu J and Zhao D M 2017 Effects of land use and cover change on the near-surface wind speed over China in the last 30 years *Prog. Phys. Geogr.* **41** 46–67

Zha J L, Wu J, Zhao D M and Fan W X 2020 Future projections of the near-surface wind speed over eastern China based on CMIP5 datasets *Clim. Dyn.* **54** 2361–85

Zha J L, Wu J, Zhao D M and Tang J P 2019 A possible recover of the near-surface wind speed in Eastern China during winter after 2000 and the potential causes *Theor. Appl. Climatol.* **136** 119–34

Zhang G F, Azorin-Molina C, Chen D L, Guijarro J A, Kong F, Minola L, McVicar T R, Son S W and Shi P J 2020 Variability of daily maximum wind speed across China, 1975–2016: an examination of likely causes *J. Clim.* **33** 2793–816

Zhang L, Li T and Lu M 2016 Trends of surface wind energy near Taiwan in winter since 1871 *Terr. Atmos. Ocean Sci.* **28** 295–302

Zhang N, Wang X M, Chen Y, Dai W and Wang X Y 2015 Numerical simulations on influence of urban land cover expansion and anthropogenic heat release on urban meteorological environment in Pearl River Delta *Theor. Appl. Climatol.* **126** 469–79

Zhang Y, Xie S P, Kosaka Y and Yang J C 2018 Pacific decadal oscillation: tropical Pacific forcing versus internal variability *J. Clim.* **31** 8265–79

Zhang Z T and Wang K C 2020 Stilling and recovery of the surface wind speed based on observation, reanalysis, and geostrophic wind theory over China from 1960 to 2017 *J. Clim.* **33** 3989–4008

Zhang Z T, Wang K C, Chen D L, Li J P and Dickinson R 2019 Increase in surface friction dominates the observed surface wind speed decline during 1973–2014 in the northern Hemisphere lands *J. Clim.* **32** 7421–35